12,05

Functionalization of $MnFe_2O_4$ magnetic nanoparticles for biomedical applications in magnetic fluid

© A.S. Kamzin[1], V.G. Semenov[2], L.S. Kamzina[1]

[1] Ioffe Institute,
St. Petersburg, Russia
[2] St. Petersburg State University,
St. Petersburg, Russia

E-mail: ASKam@mail.ioffe.ru

Received April 2, 2024
Revised June 6, 2024
Accepted June 7, 2024

The properties of magnetic nanoparticles (MNP) $MnFe_2O_4$ synthesized by the polyol method and then functionalized with 3-aminopropyltriethoxysilane (APTES) have been studied. The aim of the work is to create MNCs for magnetic fluid in biomedical applications, in particular for magnetic hyperthermic therapy of malignant tumors. The properties of the obtained particles were studied using X-ray diffraction and Mossbauer spectroscopy, which confirmed the single-phase nature of both $MnFe_2O_4$ MNP and functionalized $MnFe_2O_4$@APTES composites. From the structural analysis, it was found that the average size of the synthesized particles is ~ 13 nm, which is consistent with the data of the Messbauro studies. Magnetic and Mossbauer studies have shown that both $MnFe_2O_4$ MNPCS and $MnFe_2O_4$@APTES composites are superparamagnetic at room temperature. The functionalization (coating) of particles leads to a decrease in the effective magnetic field values compared to those observed in $MnFe_2O_4$ without coating, which is consistent with published data on a decrease in the magnetization of the $MnFe_2O_4$@APTES composite. The decrease in magnetization and effective fields is explained by the fact that when $MnFe_2O_4$ MNP is functionalized, the APTES material covers the surface layer of particles and magnetic dipole interactions decrease.

Keywords: polyol synthesis of $MnFe_2O_4$, nanoparticles, functionalization (coating) of APTES particles. The Mossbauer studies.

DOI: 10.61011/PSS.2024.07.58996.74

1. Introduction

Currently the magnetic nanoparticles for biomedicine applications are widely studied (MNP): target delivery of medicines, magneto-resonance tomography, cells separation, tissues recovery and magnetic hyperthermia. Magnetic hyperthermia (MH) treatment of malignant tumors is one of the key branches of MNP use in medicine. The MH idea is that MNP as part of magnetic fluid is entered into the target affected organ. When the external magnetic field is applied with frequency and intensity safe for a living body the MHPs are heated to the temperatures of 43−46°C and the *apoptosis* (*cell death*) of malignant cells occurs while healthy cells remain safe under these temperatures. According to the studies, the magnetic hyperthermia with the use of magnetic particles is an efficient method of treating malignant tumors [1–3]. Therefore, the search and development of MNP with biological compatibility, high heat output and limiting the heat temperature to no more than 46°C, is the key task for the researchers.

In development of MNP for biomedical applications, as well as for MH, the highest attention was paid to ferrite spinels (FS) with a general formula $M^{2+}Fe_2^{3+}O_4^{2-}$, where M^{2+} are bivalent metal ions (Ni, Cu, Co, Mn and etc.) [4–7] since, compared to iron oxides, they have higher magnetic characteristics and the better chemical stability [6,7]. Magnetic properties of the ferrite spinels are formed due to super-exchange interactions through the oxygen ions of non-equivalent tetrahedral (A) and octahedral (B) positions. These are the exchange interactions of A−B ions, as well as B−B and A−A. In this regard, it is considered that magnetic characteristics of FS can be controlled through changes in cations distribution in A and B positions using various synthesis technologies. Extensive studies of SF MNPs have demonstrated that synthesis methods have significant effect not only on particle sizes and an SF structure, but on electric, optic and magnetic SF properties, such as magnetization, anisotropy, coercive and hyperfine fields [3–7], and allow to obtain SF MNPs with required specific properties [4–13].

Manganese ferrite ($MnFe_2O_4$) among the ferrite spinels has the best characteristics for MH and provide better MRT images contrast [14,15]. These characteristics include high chemical stability, catalyst activity and specific heat capacity, wide occurrence in nature, low melting temperature and low magnetocrystalline anisotropy. High biocompatibility of Manganese ferrite is explained by the presence of ions Mn^{2+} because Manganese is required in the average amount of 2.21 mg a day for a human body [15]. Moreover, owing to high colloidal dispersability in physiological liquids the

magnetic nano-particles $MnFe_2O_4$ are especially perspective for biomedicine [4–13,16]. The key issue is the possibility of controlling the Manganese ferrite properties, using technological synthesis, and, thus, obtaining $MnFe_2O_4$ particles with the required properties.

To get the ferrite spinels MNPs of appropriate size and shape they use such methods as co-deposition, sol-gel, microwave oven, grinding in ball mill, burning, polyol and hydro-thermal methods [17]. The use of polyol method is explained by simplicity of synthesis, better particles dimensions control and dimensional distribution. In polyol method diethylene glycol often plays the role of a reducer, high-boiling solvent and stabilizer for prevention of inter-particle aggregation.

For biomedical applications and compatibility with a living body the surfaces of FS particles may be easily modified and/or appropriately functionalized [17]. Moreover, colloidal MNP mixtures and liquids are used in biomedicine. For this purpose, the MNPs are coated with a surfactant to enhance colloidal stability, minimize toxicity, prevent formation of clusters, extend the shelf life and improve compatibility between the nanoparticles and aqueous medium [17–21]. The surfactants generate a layer on the surface with efficient repulsion force between the particles, thus, improving stability in aqueous media. MNP coating material (trithoxysilane−APTES) is used due to its biocompatibility, small toxicity and presence of functional amino-groups for binding of various bioactive molecules [16–21].

Thus, there is plenty of papers for studying the impact of the coating on MNP properties. However, there are still no papers outlining the investigation of properties of the functionalized MNPs in direct comparison with those observed in the uncoated particles. Such studies could significantly expand our interpretation of modification (coating) impact on crystallographic and magnet characteristics of composites. In this regard, this paper outlines the findings of studying the properties of functionalized particles $MnFe_2O_4$@APTES in direct comparison with properties of initial MNP $MnFe_2O_4$ and influence of coating on parameters of magnetic nano-composites (MNC) $MnFe_2O_4$@APTES.

2. Synthesis of MNP $MnFe_2O_4$ and nano-composites $MnFe_2O_4$@APTES

2.1. Materials

Analytical pure chemicals such as Manganese acetate $\{Mn(CH_3COO)_2\}$, iron chloride $\{FeCl_3\}$, diethylene glycol, sodium acetate, ethanol and ethyl acetate were used in synthesis of MNP $MnFe_2O_4$ and nano-composites $MnFe_2O_4$@APTES.

2.2. Synthesis of MNP $MnFe_2O_4$

Nanoparticles $MnFe_2O_4$ were synthesized using simple low-temperature polyol method [16]. Polyol method implies a forced hydrolysis of ion metal salts in polyol, such as diethylene glycol. Diethylene glycol acts as a high boiling solvent, reducer and stabilizer inhibiting the aggregation [22,23]. For synthesis of nanoparticles $MnFe_2O_4$ the mixture of $Mn(CH_3COO)_2$ (6 mmol), $FeCl_3$ (12 mmol was dissolved in 40 mL of diethylene glycol and vigorously stirred for 20 min, after which sodium acetate was added. The resulting mixture was boiled for 3 h with reverse cooling at a temperature of 210°C. Black colloidal particles were precipitated in the round-bottom flask and cooled at room temperature. The synthesized MNP were several times washed in a mixture of ethanol and ethyl-acetate in the ratio of 1 : 2 and separated by method of magnetic decantation. The obtained MNP were dried at room temperature.

2.3. Synthesis of nano-composites $MnFe_2O_4$@APTES

To functionalize the particles and obtain $MnFe_2O_4$@APTES the surface of MNP $MnFe_2O_4$ was coated by 3-aminopropyltriethoxysilane (APTES) through the silanization reaction. For this purpose the nanoparticles $MnFe_2O_4$ were dispersed in a mixture of ethanol and water. The mixture was exposed to the action of ultrasound to get a homogeneous dispersion and 2 ml of APTES was added at a maintained temperature of 40°C in the steam chamber. After stirring of such mixture for 2 h the particles were separated by method of magnetic decantation and dried at room temperature [24].

3. Investigation techniques

X-ray diffractometer (Rigaku MiniFlex 600) with Cu-Kα ($\lambda = 1.5406$ Å) and emission range 2θ from 20 to 80° was used for the structural analysis and phase identification of obtained magnetic nanoparticles. The phase composition of the synthesized $MnFe_2O_4$ MNPs and crystallite sizes were determined by an X-ray diffraction profile using powder diffractometer (XRD Shimadzu-6100) with emission Cu-Kα and wavelength 1.542 Å.

Due to high sensitivity of Mössbauer effect to the nuclear hyperfine interactions it is possible to make an unambiguous identification of iron oxides, which have very close values of the crystal lattice constants, which is unavailable in other procedures [9,25–28]. The Mössbauer studies of the magnetic structure and phase state of the synthesized materials were carried out using a spectrometer with recording γ-quanta from the source of Co^{57}(Rh) in a sample transmission geometry. In order to measure the Mössbauer effect, the samples were packed in a plastic container so as to avoid interaction with the environment. Motion of γ-quanta ^{57}Co source with an activity of 50 mCi in the Rhodium matrix in a Doppler modulator of the spectrometer was controlled via a triangular reference signal to specify a constant-acceleration speed. The velocity scale was

calibrated by a α-Fe foil with a thickness of 6 μm at room temperature. The experimental Mössbauer spectra (MS) of $MnFe_2O_4$ MNP and $MnFe_2O_4$@APTES composites were mathematically processed by a special software [29], which describes spectrum lines by Lorentz-shaped peaks using the method of least squares. Divergence of the theoretical values of the HFI parameters is determined from the statistical deviations. The software procedure of chi-square functional minimization (χ^2) include searching optimal values of the parameters, particularly, a width, intensities and positions of the spectrum lines. Using the positions of the spectrum lines, the parameters of the hyperfine interactions (HFI) are calculated: IS — isomeric shift of Mössbauer lines, QS — quadrupole splitting, Heff — effective magnetic field.

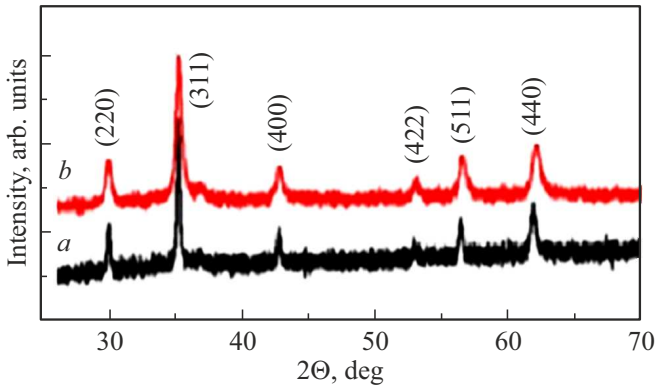

Figure 1. X-ray diffraction patterns of $MnFe_2O_4$ MNP (a) and $MnFe_2O_4$@APTES composites (b).

4. Results and discussion

4.1. X-ray diffraction analysis

X-ray diffraction patterns (XDP) of MNP $MnFe_2O_4$ and MNC $MnFe_2O_4$@APTES are shown in Figure 1. It worth noting that the obtained XRD are similar to those published for $MnFe_2O_4$ in [15,30]. The obtained values of the lattice parameter for the nanoparticles$MnFe_2O_4$ equal to 8.346 Å are consistent with the data from papers (e.g., see [31]). The diffraction peaks shown in Figure 1 correspond to the planes (220), (311), (400), (511) and (440) and indicate that the structure of studied particles corresponds to a cubic spinel $MnFe_2O_4$ and is consistent with cards JCPDS № 73-1964, JCPDS № 10-0319 and № 74-2403. Full width at half maximum (FWHM) of the most intensive peak (311) was used for calculation of the average size crystallites of magnetic nanoparticles from Scherrer formula [32,33]. From the analysis we may see that the size of crystallites $MnFe_2O_4$ is 8−10 nm, which is consistent with findings from paper [16].

XRD (Figure 1) prove that the reverse spinel (Fd3m) has cubic structure for both samples. The lattice constant was 8.346 Å and was calculated allowing for single phase for both samples. From the X-ray patterns we may make a conclusion that APTES coating doesn't influence the crystallite structure of particles $MnFe_2O_4$. However, in case of composites $MnFe_2O_4$@APTES the widths of lines are higher than for $MnFe_2O_4$, and intensities go down.

4.2. Experimental Mössbauer spectra of MNP $MnFe_2O_4$ and MNC $MnFe_2O_4$@APTES

Mössbauer spectroscopy (MSp) — a unique method based on non-redundant resonant absorption of γ emission is a probe for both, the structure and magnetism at the local level [25–28]. High selectivity of MSp to Fe^{2+} and Fe^{3+} ions, to the environment of Fe atoms, allows extracting information about the structure, valence state, stoichiometry, types of coordination and magnetic ordering, phase transitions and phase components. MSp unambiguously identifies iron oxides (hematite, magnetite, maghemite, etc.), which is not available for other known methods. The short measurement time 10^{-8} s) makes the MSp sensitive to the relaxation effects.

Mössbauer spectra (MS) registered at 300, 80 and 300 K with imposition of external magnetic field for $MnFe_2O_4$ MNP and $MnFe_2O_4$@APTES composites are given in Figure 2. As we may see in Figure 2 the Mössbauer spectra are composed of wide lines of Zeeman sextuplets (ZS), the intensity of which decreases towards zero speed, thus, significantly complicating the analysis of experimental spectra. Therefore, to process the experimental MS of MNP and composites we used matching of model components with experimental values [29]. Analysis of MS makes it possible to find the components of sextuplets (and doublets) and draw conclusions about the belonging of these components to the corresponding iron oxides and positions of Fe ions in the crystal lattice [25–28]. The difference between the experimental and model values is minimal and is shown above each spectrum. Deviation value (χ^2) of the model components used to describe experimental MS determines the accuracy of matching, which in our cases was in the range from 1.1 to 1.2, which indicates a good match of the models used with experimental data and, consequently, the reliability of such processing. The experimental values of MS (Figure 2) are shown by dots, and the model components obtained by mathematical processing of MS using dedicated program [29] are shown by solid lines. By using positions of spectral lines of MS in MNP $MnFe_2O_4$ and MNC $MnFe_2O_4$@APTES the parameters of hyperfine interactions (HFI) were analyzed: isomeric shifts (IS), quadruple splits (QS), effective fields (Heff), given in Tables 1 and 2, respectively. Restored from MS (Figure 2) the probability functions of distribution of effective magnetic fields $P(H\text{eff})$ are given in Figure 3.

In Mössbauer spectroscopy Fe^{3+} and Fe^{2+} ions are unambiguously identified by their chemical shifts which make $\sim 0.2 \div 0.5$ mm/s and $\sim 0.9 \div 1.1$ mm/s, respectively [34]. Table 2 shows that the values of IS are within the range

Table 1. The widths of the first and sixth lines (G) of Zeeman splitting, as well as values of isomer shifts (IS), quadrupolar splitting (QS), effective magnetic fields (*H*eff) and areas of components (In) for Fe ions in tetrahedral (A) and octahedral (B) positions and doublets (D) in MNP $MnFe_2O_4$, at $T = 300$ K and 80 K, as well as at 300 K in the external magnetic field with intensity 0.17 T

$MnFe_2O_4$At	Components	G (mm/s)	IS (mm/s)	QS (mm/s)	*H*eff (T)	In (%)
300 K	A	0.372 + / − 0.000	0.339 + / − 0.007	0.010 + / − 0.014	49.43 + / − 0.06	8
	B1	0.488 + / − 0.053	0.330 + / − 0.005	0.007 + / − 0.009	47.76 + / − 0.07	16
	B2	0.734 + / − 0.112	0.371 + / − 0.007	0.012 + / − 0.014	45.30 + / − 0.19	20
	S	1.390 + / − 0.091	0.417 + / − 0.015	0.024 + / − 0.026	40.84 + / − 0.31	40
	D	1.180 + / − 0.119	0.338 + / − 0.010	0.722 + / − 0.029	–	16
80 K	A	0.460 + / − 0.028	0.398 + / − 0.005	0.008 + / − 0.011	50.67 + / − 0.07	17
	B1	0.509 + / − 0.000	0.370 + / − 0.005	0.002 + / − 0.010	48.82 + / − 0.07	20
	B2	0.576 + / − 0.000	0.394 + / − 0.010	0.009 + / − 0.021	46.22 + / − 0.13	13
	S	1.418 + / − 0.154	0.494 + / − 0.020	0.025 + / − 0.036	42.06 + / − 0.36	44
	D	0.790 + / − 0.127	0.416 + / − 0.022	0.665 + / − 0.049	–	7
300 K In MF	A	0.388 + / − 0.000	0.336 + / − 0.005	0.010 + / − 0.010	49.04 + / − 0.04	15
	B1	0.528 + / − 0.000	0.333 + / − 0.007	0.003 + / − 0.014	47.33 + / − 0.06	21
	B2	0.819 + / − 0.000	0.360 + / − 0.019	0.070 + / − 0.037	44.06 + / − 0.11	18
	S	1.730 + / − 0.152	0.465 + / − 0.027	0.014 + / − 0.044	38.95 + / − 0.38	41
	D	0.935 + / − 0.245	0.230 + / − 0.034	0.707 + / − 0.093	–	5

Table 2. The widths of the first and sixth lines (G) of Zeeman splitting, as well as values of isomer shifts (IS), quadrupolar splitting (QS), effective magnetic fields (*H*eff) and areas of Zeeman sextiplets (S) for Fe ions in tetrahedral (A) and octahedral (B) positions and doublets (D) in composite $MnFe_2O_4$@APTES at $T = 300$ K and 80 K, as well as at 300 K in the external magnetic field with an intensity of 0.17 T

$MnFe_2O_4$@APTES at	Components	G (mm/s)	IS (mm/s)	QS (mm/s)	*H*eff (T)	In (%)
300 K	A	0.501 + / − 0.000	0.319 + / − 0.006	0.031 + / − 0.011	48.88 + / − 0.05	14
	B1	0.594 + / − 0.000	0.321 + / − 0.006	0.027 + / − 0.012	46.59 + / − 0.08	17
	B2	0.677 + / − 0.000	0.342 + / − 0.009	0.033 + / − 0.019	43.32 + / − 0.11	13
	B3	0.896 + / − 0.000	0.993 + / − 0.024	1.276 + / − 0.043	39.63 + / − 0.20	9
	S	1.969 + / − 0.000	0.488 + / − 0.050	0.391 + / − 0.096	36.50 + / − 0.36	45
	D	0.520 + / − 0.105	0.016 + / − 0.030	0.377 + / − 0.055	–	2
80 K	A	0.391 + / − 0.000	0.396 + / − 0.012	0.006 + / − 0.023	51.09 + / − 0.10	13
	B1	0.444 + / − 0.000	0.377 + / − 0.009	0.029 + / − 0.018	49.18 + / − 0.11	19
	B2	0.547 + / − 0.000	0.354 + / − 0.020	0.009 + / − 0.040	46.65 + / − 0.26	12
	S	1.796 + / − 0.261	0.397 + / − 0.035	0.063 + / − 0.059	44.38 + / − 0.67	54
300 K In MF	A	0.446 + / − 0.000	0.339 + / − 0.014	0.036 + / − 0.029	48.93 + / − 0.06	19
	B1	0.489 + / − 0.000	0.334 + / − 0.009	0.049 + / − 0.018	46.75 + / − 0.10	22
	B2	0.659 + / − 0.000	0.196 + / − 0.019	0.173 + / − 0.039	43.89 + / − 0.18	17
	S	1.448 + / − 0.000	0.406 + / − 0.023	0.088 + / − 0.043	39.55 + / − 0.30	43

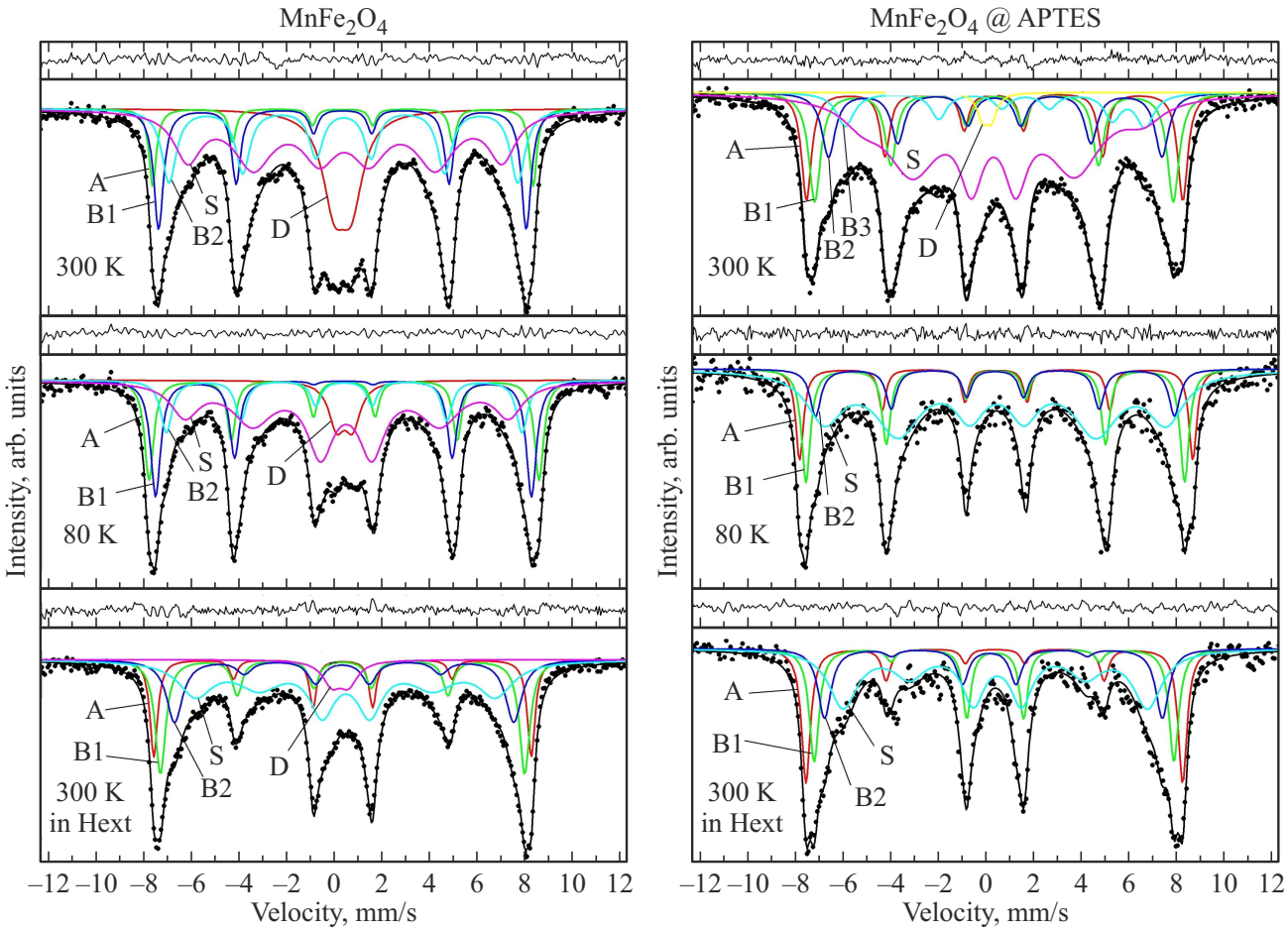

Figure 2. Mössbauer spectrum of MNP $MnFe_2O_4$ and MNC $MnFe_2O_4$@APTES obtained at 300 and 80 K, as well as at 300 K in the externa magnetic field with intensity of 0.17 T. The dots show experimental values, while model components are shown with solid lines.

of $0.2 \div 0.4$ mm/s, indicating that in the studied MNP only Fe^{3+} ions are present in the high-spin state.

The impurity phases of the iron oxides should appear distinctly on MS as additional Zeeman sextuplets (ZS) or doublets with different HFI parameters. The detection limit of the secondary phase is about 3 at.% of the iron and any impurity phase even with such an iron quantity can be easily determined from the Mössbauer spectra. The analysis of experimental Mössbauer spectra of the studied particles (Figure2) has not revealed any additional lines. Thus, there are no impurity phases in the MNPs under study, which coincides with results of Raman studies [16] and XRD (Figure 1).

4.3. Experimental Mössbauer spectra of MNP $MnFe_2O_4$ and MNC $MnFe_2O_4$@APTES in the absence of external magnetic field

The Mössbauer spectra (MS) of MNP $MnFe_2O_4$ obtained at room temperature without imposition of a magnetic field are shown in Figure 2. It should be noted that the experimental spectra of MNP $MnFe_2O_4$ at room temperature are equivalent to those mentioned in papers [35–39]. The crystalline structure of ferrite spinels consists of two non-equivalent positions of Fe ions and the Mössbauer spectrum of FS shall be delineated by two ZS belonging to Fe ions in these positions. However, experimental MS of FS are not delineated by such model. Therefore, the observed broadening of the ZS lines in MS of ferrite spinels towards zero rates was explained by the random distribution of cations by (A) nodes which resulted in formation of several octahedral [B] positions different in occupation density [40,41]. Fe ions in (A) nodes of FS have twelve closest neighbors in [B] positions, therefore they less depend on random distribution of cations across [B] positions. Fe ions in [B] positions have only six neighboring cations occupying (A) nodes, therefore any random distribution of magnetic cations in (A) nodes has a much more influence on effective fields of Fe [B] ions of the sub-lattice [40]. Based on the above, in MNP $MnFe_2O_4$ and MNC $MnFe_2O_4$@APTES (Figure 2) Zeeman sextuplet with the highest effective field was attributed to Fe ions occupying (A) positions in FS crystalline lattice, while sextuplets with lower values Heff — were attributed to Fe ions in [B] positions.

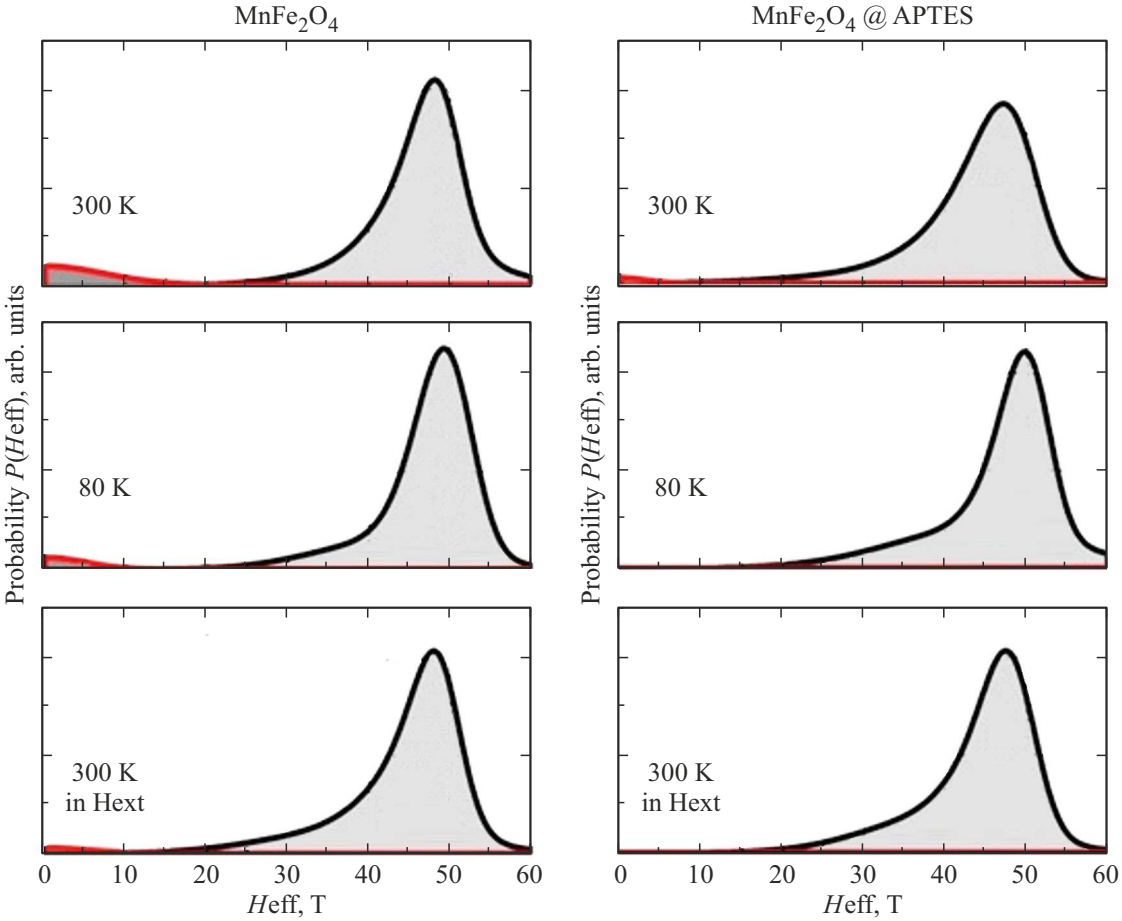

Figure 3. Distribution functions of effective magnetic fields P (Heff) in MNP $MnFe_2O_4$ and LSM $MnFe_2O_4$@APTES restored from experimental spectra of MNP $MnFe_2O_4$ and MNC $MnFe_2O_4$@APTES using software [29].

On experimental MS of MNP $MnFe_2O_4$ the lines of paramagnetic phase with intensity of 16% at 300 K, and 7% at 80 K were observed, while on MS of MNC $MnFe_2O_4$@APTES the intensity of such line is reduced to 2% at 300 K, and at 80 K it goes down to zero. Formation of paramagnetic phase lines can be explained by oxidation of particles$MnFe_2O_4$ within the period of time from synthesis to Mössbauer measurements. $MnFe_2O_4$ particles were functionalized directly after their synthesis, and, hence, APTES layer on the surface of particles protects MNP from oxidaton.

The values of effective fields of the functionalized MNC$MnFe_2O_4$@APTES are lower than the values obtained for MNP $MnFe_2O_4$, which is explained by the influence of coating on the properties of $MnFe_2O_4$ particles. The reduced magnetic moment can be interpreted as the influence of the fine non-magnetic surface layer [42]. Reduced effective fields are consistent with the decrease of composites magnetization $MnFe_2O_4$@APTES, observed in [16]. As seen from 2, total width of Zeeman component on MS of the composites$MnFe_2O_4$@APTES is higher than that for $MnFe_2O_4$ particles. Apparently, due to the particles coating they are separated by the surface layer and both, their mechanical and magnetic bonds between MNP become loose [42]. This results in enhancement of relaxation effects [43]. We may suggest that magnetic blocking occurs not because of super-paramagnetic relaxation of the non-interacting particles but due to ordering of the interacting magnetic moments.

Apart from ZS, belonging to Fe ions in (A) and [B] positions, on MS (Figure 2) we may see the sextuplets with sufficiently high widths of the lines (Table 1) and lower Heff values, than for (A) and [B] ions. Similar MS were observed in [34–39,44–51], however, the way such sextuplet was formed was explained differently. In [44] the sextuplets with significantly larger widths of Zeeman lines were attributed to small accumulations of Fe ions during grinding, but no signs of such an accumulation were observed on the XRD. The occurrence of a sextuplet of S type is explained by the distribution of Fe and Mn ions over the sub-lattices [45] or by relaxation effects in [44–48]. The Mössbauer spectra of magnetite featuring Zeeman sextuplet with wide lines were delineated by the use of three sextuplets [52], two of which were linked with A and B positions. The formation of third sextuplet with low effective magnetic field was explained by potential magnetic interactions between the particles.

When moving from macro-crystals to the nanoscale particles the surface/volume ratio significantly rises. Thus, there are approximately 0.15, 20 and 60% of the atoms of the composition, respectively, in particles with a diameter of 1 μm, 6 nm and 1.6 nm on the surface [53]. Thus, in formation of MNP properties the role of Fe ions located in the surface layer of particles becomes more essential. This is the reason for significant differences between the MS of large and small particles [54–56] and, as suggested in [57,58], it can form spin-glass or „dead-magnetic" phase.

Thus, the sextuplet observed on MS, with the lines width much higher compared to the other lines, was explained by exclusive role of the surface. The existence of an anisotropic layer on the surface in ferromagnetic crystals was theoretically predicted by L. Neel in 1954. [59]. Experimental studies of the properties of the surface layer attracted attention much later (see [60,61] and references), and the studies were conducted on thin films and nanoscale powders, because the surface/volume ratio in these materials is increased multiply and the surface spins of Fe ions become dominant in formation of the film or particle properties in whole. The first evidence of the skewed state phenomenon of spin moments in particles was obtained in Mössbauer studies in strong magnetic fields [25,62]. Further, the surface properties were studied using thin powders or films [25]. However, such studies are extremely complicated, because, for instance, the particles are non homogenous in dimensions and depend on the fabrication technology and etc.

New unique opportunities for studying the properties of macroscopic crystals appeared due to the method of „simultaneous gamma, X-ray and electron Mossbauer spectroscopy (SGXEMS)", first proposed and implemented in [63–65]. The uniqueness of the SGXEMS method is that information about the state of the surface layer and the volume of the crystal is extracted simultaneously using the same technique (Mössbauer spectroscopy). This allows a direct comparison of experimental data of the properties of the surface and the volume of the crystal. Later, the SGXEMS method in foreign literature was called „Simultaneous Triple Radiation Mössbauer Spectroscopy (STRMS)" [66,67]. It was SGXEMS method that first proved the existence in Fe_3BO_6 crystals of a surface layer where, when approaching the surface, the magnetic moments of Fe ions change their orientation [60,61]. This layer was called a „transit layer" [60,61]. Using SGXEMS method such „transit" surface layer was identified in hexagonal ferrites $BaFe_{12-x}Sc_xO_{19}$ and $SrFe_{12-x}Al_xO_{19}$, where part of Fe ions was substituted by the diamagnetic Sc and Al ions, respectively. The input of diamagnetic ions result in additional (present due to the surface) breakage of super-exchange bonds [68–72]. Consequently, the surface and diamagnetic ions lead to significant changes in the super-exchange interactions of Fe ions occupying positions in the surface and near-surface layers. It can be argued that moments orientation offset from the direction in volume observed in the surface layer of macrocrystals should be preserved when the size of the macrocrystals decreases to nanowires.

The large line widths of S component suggest that the S sextuplet is formed by Fe ions located on the surface and in the near-surface layer of MNP, in which the presence of the surface led to the loss of more magnetic neighbors and, consequently, super-exchange bonds than in the ions in the particle volume. An additional contribution to the sextuplet S may come from the same Fe ions of the surface and near-surface layer, which, due to the loss of part of the super-exchange interactions, are transformed into the super-paramagnetic state at temperatures lower than the ions in the volume of the particle.

It should be noted that the state with different magnetic structures of the volume and the surface layer in the SF MNP cannot be observed by other methods other than Mössbauer spectroscopy. This is explained by the fact that SF MNP are single-phase, well crystallized, and consist of a single material. This distinguishes SF particles from core/shell composites, in which the core and shell are made of different magnets, for example, magnetite and maghemite [73].

4.4. Mössbauer studies of MNP $MnFe_2O_4$ and composites $MnFe_2O_4$@APTES at room temperature in the external magnetic field with a strength of 0.17 T

The use of external magnetic fields allowed to significantly broaden the knowledge obtained through Mössbauer spectroscopy. Due to Mössbauer measurements in the strong external magnetic fields (EMF), with a strength of dozens of kOe, the direct evidence was obtained concerning existence in MNP of a skewed structure of magnetic moments of Fe ions [25,74,75] as described by Yapheth-Kittel model [76]. The data on distribution of ions in FS sub-lattices also can be obtained from the Mössbauer studies in strong EMF [25].

The importance of studies of weak magnetic fields (units of kOe or less) influence on MNP properties, that started in late 60s [77,78] is necessitated by the need of investigating the MNP properties impacted by weak external magnetic fields used in hyperthermia treatment of malignant tumors [18]. In theoretical insights, it was shown that the Mössbauer spectroscopy with the superimposition of weak EMFs (with a strength of hundreds Oe) allows us to study the dynamic effects associated with the processes of fluctuation of the magnetic moment and transition to the paramagnetic state, since EMF stabilizes the ultrafine structure of a superparamagnet and increases the spin relaxation time (see, for example, [43,57,79]).

Figure 2 shows the MS of MNP$MnFe_2O_4$ and MNC $MnFe_2O_4$@APTES obtained at room temperature in the external magnetic field with a strength of 0.17 T, oriented parallel to the gamma-emission beam. From experimental MS of the studied particles given in Figure 2, we calculated the HFI parameters given in Tables 1 and 2.

As seen from Figure 2, when EMF is imposed on MS a significant decrease in intensity of the first and fifth ZS lines is observed, because EMF is oriented parallel to the gamma-radiation beam. Large widths of MS lines of the studied particles in EMF also imply the distribution of Heff, because of different environment of Fe^{3+} ions. The imposition of a magnetic field with a strength of 0.17 T leads to stabilization, but not to complete suppression of superparamagnetic behavior in the studied samples.

The presence on MS, obtained in magnetic fields of both, MNP $MnFe_2O_4$, and MNC $MnFe_2O_4$@APTES, of the lines denoted as S, also indicates that the studied particles have a core/shell type structure as outlined above. At that, these particles are in a superparamagnetic state, which is required for hyperthermic treatment of malignant tumors.

On the MS of the functionalized particles $MnFe_2O_4$@APTES as well as $MnFe_2O_4$ particles there is observed an asymmetric increase of the lines widths of rates zero (Figure 2), however, as can be seen from Tables 1 and 2, the values Heff for the functionalized particles at room temperature were reduced. The functionalized $MnFe_2O_4$ particles as was found in [16] result in decrease of saturation magnetization (Ms), similar to Heff. This is due to the fact that the coating of particles makes them isolated from each other, and, hence, leads to loosened exchange interactions between the particles, decreased effective fields and enhanced relaxation effects.

4.5. Analysis of distribution functions Heff of $MnFe_2O_4$ MNP and $MnFe_2O_4$@ MNC APTES

Because of local inhomogeneities of the cations distribution the sextuplets with Zeeman lines resolution are absent on MS. At that, the use of Lorentz lines in the analysis of curves of effective magnetic fields $P(H\text{eff})$ distribution is not efficient. In such cases, the most reliable method is MS processing using the Voigt function as a spectral line [80,81], Therefore, to restore $P(H\text{eff})$ function from experimental MS the Voigt function was used as a spectral line in program [29]. The probability functions of effective magnetic fields $P(H\text{eff})$ distribution, obtained from experimental MS, are shown in Figure 3.

Comparison of dependencies of hyperfine magnetic fields (Heff) distribution in samples with coating and in uncoated samples under various measurement conditions enables us to make the following conclusions. An uncoated sample is featuring not only a narrower distribution of hyperfine magnetic fields, but the maximum of their distribution is shifted towards higher magnetic fields. This can be explained by the fact that the functionalized composites $MnFe_2O_4$@APTES are isolated from each other by a coating layer which leads to loosened exchange interactions between the particles, decreased effective fields and enhanced relaxation effects.

The observed maximum in the area of small fields corresponds to the paramagnetic phase and its share is the highest for the uncoated particles. This contribution can be interpreted as a share of Fe ions in the paramagnetic state in the surface layer of uncoated particles formed on the surface of initial particles during absorption of oxygen, hydrogen and carbon atoms. This layer prevents the particle volume from further oxidation. At the same time the distribution functions Heff for coated particles have a narrower distribution compared to MNP$MnFe_2O_4$, and full absence of the paramagnetic component.

Wider distribution of hyperfine magnetic fields for the uncoated particles can be explained by the presence of higher thermal fluctuations of Fe ions magnetic moments, the fluctuation rate of which is comparable with life period of the core in excited state ($\sim 10^{-8} \div 10^{-9}$ s). This conclusion is well proved by measurements at the temperature of liquid nitrogen (Figure 2). In this case the distributions of the hyper-fine structure practically coincide. This indicates an extensive attenuation of thermal fluctuations (perturbations). Though, for the uncoated particles there still remains the paramagnetic component, however it is significantly reduced. This may imply the stabilization of the particle's magnetic system by the action of external magnetic field and the growth of magnetic component influence from the „core" of the particle to the near-surface layer.

Measurements with application of at least a small outer magnetic field ($H \sim 0.17$ T) would have demonstrated how the induced magnetic anisotropy impacts the thermal fluctuations stabilization even at a temperature of 300 K (Figure 2). It turned out that outer magnetic field stabilizes the particles magnetic system no worse than the influence of particles cooling down to a temperature of 80 K.

5. Conclusion

The nanoparticles $MnFe_2O_4$ and functionalized nanocomposites $MnFe_2O_4$@APTES obtained by polyol method have been studied to understand the mechanism of coating effect on MNP properties and to develop the liquid-dispersible surface-modified bio-compatible magnetic nanoparticles for the biomedicine purposes.

X-ray diffraction patterns and Mössbauer spectra showed that both, the synthesized MNPs $MnFe_2O_4$ and the composites $MnFe_2O_4$@APTES are single-phase and have no foreign impurities. The coating leads to reduction of effective magnetic fields (Heff), which is consistent with the decrease of saturation magnetization (Ms) observed in [16]. Presence of coatings on particles $MnFe_2O_4$ was proved by Raman-scattering spectroscopy [16]. Decrease of Heff and Ms saturation of composite $MnFe_2O_4$@APTES is explained by the fact that APTES covers the surface layer of particles and results in attenuation of magnetic dipole interactions. It is established that $MnFe_2O_4$@APTES composites are in the super-magnetic state and have high saturation magnetization and, as shown in [16], feature maximal specific absorption rate because the molecules of APTES surface layer separate the particles reducing both, the mechanical and magnetic bonds between the particles. Thus, the functionalized MNP and formed nano-composites

$MnFe_2O_4$@APTES are perspective for use as heat sources in magnetic hyperthermia treatment of malignant tumors even at low concentration of particles in magnetic liquid.

Conflict of interest

The authors declare that they have no conflict of interest.

References

[1] S.R. Patade, D.D. Andhare, S.B. Somvanshi, S.A. Jadhav, M.V. Khedkar, K.M. Jadhav. Ceram. Int. **46**, *16*, Pt. A, 25576 (2020). https://doi.org/10.1016/j.ceramint.2020.07.029

[2] A. Baki. F. Wiekhorst, R. Bleul. Bioengineering **8**, 134 (2021). https://doi.org/10.3390/bioengineering8100134.

[3] Clinical Applications of Magnetic Nanoparticles / Ed. Nguyen T.K. Thanh. CRC Press Taylor & Francis Group (2018). P. 495.

[4] M.M. Cruz, L.P. Ferreira, J. Ramos, S.G. Mendo, A.F. Alves, M. Godinho, M.D. Carvalho. J. Alloys Comp. **703**, 370 (2017). https://doi.org/10.1016/j.jallcom.2017.01.297

[5] B. Aslibeiki, P. Kameli, H. Salamati, G. Concas, M.S. Fernandez, A. Talone, G. Muscas, D. Peddis. Beilstein J. Nanotechnol. **10**, 856 (2019).

[6] K. Islam, M. Haque, A. Kumar, A. Hoq, F. Hyder, S.M. Hoque. Nanomaterials **10**, 2297 (2020).

[7] V. Narayanaswamy, I.A. Al-Omari, A.S. Kamzin, B. Issa, H.O. Tekin, H. Khourshid, H. Kumar, A. Mallya, S. Sambasivam, I.M. Obaidat. Nanomaterials **11**, 1231 (2021).

[8] X. Wang, X. Kan, X. Liu, S. Feng, G. Zheng, Z. Cheng, W. Wang, Z. Chen, C. Liu. Mater. Today Commun. **25**, 101414 (2020).

[9] A.S. Kamzin. V.G. Semenov, I.A. Al-Omari, V. Narayanaswamy, B. Issa. Phys. Solid State **65**, *8*, 1363 (2023). DOI: 10.61011/PSS.2023.08.56586.122.

[10] K.M. Srinivasamurthy, V.J. Angadi, S.P. Kubrin, S. Matteppanavar, D.A. Sarychev, P. Mohan Kumar, H.W. Azale, B. Rudraswamy. Ceram. Int. **44**, 9194 (2018).

[11] F.G. da Silva, J. Depeyrot, A.F.C. Campos, R. Aquino, D. fiorani, D. Peddis. J. Nanosci. Nanotechn. **19**, 4888 (2019).

[12] T. Dippong, E.A. Levei, O.C. Goga, D. Toloman. G. Borodi. J. Therm. Anal. Calorimetry **136**, 1587 (2019).

[13] A. Manohar, D.D. Geleta, C. Krishnamoorthi, J. Lee. Ceram. Int. **46**, 28035 (2020).

[14] C.R. Alves, R. Aquino, J. Depeyrot, F.A. Tourinho, E. Dubois, R. Perzynski. J. Mater. Sci. **42**, 2297 (2007). DOI: 10.1007/s10853-006-0601-y

[15] R.M. Tripathi, S. Mahapatra, R. Raghunath, V.N. Sastry, T.M. Krishnamoorthy. Sci. Total Environ **250**, 43 (2000).

[16] P.R. Ghutepatil, A.B. Salunkhe, V.M. Khot, S.H. Pawar. Chem. Papers **73**, 2189 (2019). https://doi.org/10.1007/s11696-019-00768-z

[17] G. Kandasamy. Nanotechnology **30**, *50*, 502001 (2019). https://doi.org/10.1088/1361-6528/ab3f17

[18] A.K. Gupta, M. Gupta. Biomaterials **26**, 3995 (2005).

[19] E.A. Smith, W. Chen. Langmuir **24**, 12405 (2008).

[20] M.H. Mashhadizadeh, M. Amoli-Diva. J. Nanomed. Nanotechol. **3**, 139 (2010).

[21] B. Cortis-Llanos, S.M. Ocampo, L. de la Cueva, G.F. Calvo, J. Belmonte-Beitia, L. Pirez, G. Salas, A. Ayuso-Sacido. Nanomaterials **11**, 2888 (2021). https://doi.org/10.3390/nano11112888

[22] W. Cai, J. Wan. J. Colloid. Interface Sci. **305**, 366 (2007).

[23] Z. Beji, A. Hanini, L.S. Smiri, J. Gavard, K. Kacem, F. Villain, J.M. Grenéche, F. Chau, S. Ammar. Chem. Mater. **22**, 5420 (2010).

[24] A. Ebrahiminezhad, Y. Ghasemi, S. Rasoul-Amini, J. Barar, S. Davarana. Colloids Surf. B **102**, 534 (2013).

[25] Mössbauer Spectroscopy Applied to Magnetism and Material Science / Eds. G.J. Long, F. Grandjean.Plenum Press, N.Y. (1993). 479 p.

[26] Ferrite Nanostructured Magnetic Materials Technologies and Applications Ed. J.P. Singh, K.H. Chae, R.C. Srivastava, O.F. Caltun. Woodhead Publishing (2023). 926 p.

[27] A.S. Kamzin, I.M. Obaidat, V.G. Semenov, V. Narayanaswamy, I.A. Al-Omari, B. Issa, I.V. Buryanenko. Phys. Solid State **65**, *3*, 470 (2023). DOI: 10.21883/PSS.2023.03.55591.544.

[28] A.S. Kamzin, V.G. Semenov, L.S. Kamzina. FTT **66**, *3*, 482 (2024). (in Russian).

[29] V.G. Semenov, V.V. Panchuk. The Mössbauer Spectra Processing MossFit software. Chast. soobschenie.

[30] C. Pereira, A. M. Pereira, C. Fernandes, M. Rocha, R. Mendes, M.P. Fernández-García, A. Guedes, P.B. Tavares, J-M. Greneéche, J.P. Araújo, C. Freire. Chem. Mater. **24**, 1496 (2012).

[31] C.V. Ramana, Y.D. Kolekar, K.K. Bharathi, B. Sinha, K. Ghosh. J. Appl. Phys. **114**, 183907 (2013).

[32] P. Scherrer. Göttinger Nachrichten Gesell **2**, 98 (1918).

[33] A. Patterson. Phys. Rev. **56**, *10*, 978 (1939). DOI: 10.1103/PhysRev.56.978

[34] A.S. Kamzin, G. Caliskan, N. Dogan, A. Bingolbali, V.G. Semenov, I.V. Buryanenko. Phys. Solid State **64**, *10*, 1559 (2022). DOI: 10.21883/PSS.2022.10.54249.391.

[35] Y.H. Li, T. Kouh, I.B. Shim, Ch.S. Kim. J. App. Phys. **111**, 07B544 (2012). DOI: 10.1063/1.3687007

[36] B. Kalska, J.J. Paggel, P. Fumagalli, J. Rybczynski, D. Satula, M. Hilgendorff, M. Giersig. J. App. Phys. **95**, 1343 (2004). DOI: 10.1063/1.1637134

[37] S.K. Shaw, J. Kailashiya, Santosh K. Gupta, C.L. Prajapat, Sher Singh Meena, D. Dash, P. Maitig, N.K. Prasada. J. All. Comp. **899**, 163192 (2022). https://doi.org/10.1016/j.jallcom.2021.163192

[38] M. Popa, P. Bruna, D. Crespo, M. Jose, C. Moreno. J. Am. Ceram. Soc., **91**, *8*, 2488 (2008). DOI: 10.1111/j.1551-2916.2008.02501.x

[39] A. Yang, C.N. Chinnasamy, J.M. Greneche, Y. Chen, S.D. Yoon, Z. Chen, K. Hsu, Z. Cai, K. Ziemer, C. Vittoria, V.G. Harris. Nanotechnology **20**, 185704 (2009). DOI: 10.1088/0957-4484/20/18/185704

[40] G.A. Sawatzky, F. Van Der Woude, A.H. Morrish. J. Appl. Phys. **39**, 1204 (1968).

[41] G.A. Sawatzky, F. Van Der Woude, A.H. Morrish. Phys. Rev. **187**, 747 (1969).

[42] A.H. Morrish, K. Haneda, J. Magn. Magn. Mater. **35**, 105 (1983).

[43] S. Morup, C.A. Oxborro, P.V. Hendriksen, M.S. Pedersen, M. Hanson, C. Johansson. J. Magn. Magn. Mater. **140–144**, 409 (1995).

[44] W.B. Dlamini, J.Z. Msomi, T. Moyo. J. Magn. Magn. Mater. **373**, 78 (2015). http://dx.doi.org/10.1016/j.jmmm.2014.01.066
[45] Y.H. Li, T. Kouh, I.-B. Shim, Ch.S. Kim. J. App. Phys. **111**, 07B544 (2012). DOI: 10.1063/1.3687007
[46] S. Morup, H. Topsoe. App. Phys. **11**, 63 (1976).
[47] M.A. Chuev. ZhETF **141**, 698 (2012). (in Russian).
[48] Magnetic Spinels — Synthesis, Properties and Applications. Ed. M.S. Seehra. 2017. doi:10.5772/63249. Perales-Pérez, O., & Cedefo-Mattei, Y. Optimizing Processing Conditions to Produce Cobalt Ferrite Nanoparticles of Desired Size and Magnetic Properties. Ch. 3. 2017. http://dx.doi.org/10.5772/66842.
[49] K.L. Zaharieva, Z.P. Cherkezova-Zheleva, B.N. Kunev, I.G. Mitov, S.S. Dimova. Bulgar. Chem. Commun. **47**, 261 (2015).
[50] S.B. Singh, Ch. Srinivas, B.V. Tirupanyam, C.L. Prajapat, M.R. Singh, S.S. Meena, Pramod Bhatte, S.M. Yusuf, D.L. Sastry. Ceram. Int. **42**, 19188 (2016). http://dx.doi.org/10.1016/j.ceramint.2016.09
[51] A. Alomari, H.M. El Ghanem, A.-F. Lehlooh, I.M. Arafa, I. Bsoul. Sensors & Transducers **192**, 53 (2015).
[52] J.A. Celis, O.F. Olea Mejıa, A. Cabral-Prieto, I. Garcıa-Sosa, R. Derat-Escudero, E.M. Baggio-Saitovitch, M. Alzamora Camarena. Hyperfine Interact. **238**, 43 (2017). DOI: 10.1007/s10751-017-1414-x
[53] B. Issa, I. Obaidat, B. Albiss, Y. Haik. Int. J. Mol. Sci. **14**, 21266 (2013). http://www.mdpi.com/1422-0067/14/11/21266
[54] T. Muthukumaran, S.S. Pati, L.H. Singh, A.C. de Oliveira, V.K. Garg. J. Philip. App. Nanosci **8**, 593 (2018). https://doi.org/10.1007/s13204-018-0715-y
[55] R. Ghosh, L. Pradhan, Y.P. Devi, S.S. Meena, R. Tewari, A. Kumar, S. Sharma, N.S. Gajbhiye, R.K. Vatsa, B.N. Pandey, R.S. Ningthoujam. J. Mater. Chem. **21**, 13388 (2011).
[56] M.I.A.A. Maksoud, A. El-Ghandour, G.S. El-Sayyad, R.A. Fahim, A.H. El-Hanbal, M. Bekhit, E.K. Abdel-Khale, H.H. El-Bahnasawy, M.A. Elkodous, H. Ashour, A.S. Awed. J. Inorg. Organomet. Polym. Mater. **30**, 3709 (2020). https://doi.org/10.1007/s10904-020-01523-8
[57] S. Mørup, F. Bødker, P.V. Hendriksen, S. Linderoth. Phys. Rev. B **52**, 287 (1995).
[58] A.E. Berkowitz, W.J. Schuele, P.J. Flanders, J. Appl. Phys. **39**, 1261 (1968). DOI: 10.1103/physrevlett.27.1140
[59] L. Neel. J. Phys. Rad. **15**, *4*, 225 (1954).
[60] A.S. Kamzin, L.A. Grigor'ev. JETP Lett. **57**, *9*, 557 (1993).
[61] A.S. Kamzin, L.A. Grigor'ev. ZETP **77**, *4*, 658 (1993).
[62] J.M.D. Coey. Phys. Rev. Lett. **27**, *17*, 1140 (1971).
[63] A.S. Kamzin, V.P. Rusakov, L.A. Grigoriev. Int. Conf. USSR. Proceed. Part II, 271 (1988).
[64] A.S. Kamzin, L.A. Grigor'ev. Sov. Tech. Phys. Lett. **6**, *6*, 417 (1990).
[65] A.S. Kamzin, L.A. Grigor'ev. Sov. Tech. Phys. **35**, *7*, 840 (1990).
[66] F. Schaaf, U. Gonser. Hyperfine Interact. **57**, *1–4*, 2101 (1990).
[67] U. Gonzer, P. Schaaf, F. Aubertin. Hyperfine Interact. **66**, *1–4*, 95 (1991).
[68] A.S. Kamzin, L.P. Ol'khovik, V.L. Rozenbaum. JETP **84**, *4*, 788 (1997).
[69] A.S. Kamzin. JETP **89**, *5*, 891 (1999).
[70] A.S. Kamzin, L.P. Ol'khovik, V.L. Rozenbaum. Phys. Solid State **41**, *3*, 433 (1999).
[71] A.S. Kamzin, V.L. Rozenbaum, L.P. Ol'khovik. JETP Lett. **67**, *10*, 843 (1998).
[72] A.S. Kamzin, L.P. Ol'khovik. Phys. Solid State **41**, *10*, 1658 (1999).
[73] A.S. Kamzin, I.M. Obaidat, A.A. Valiullin, V.G. Semenov, I.A. Al-Omari. Phys. Solid State **62**, *10*, 1933 (2020). DOI: https://link.springer.com/article/10.1134/S1063783420100157.
[74] K. Haneda, A.H. Morrish. J. Appl. Phys. **63**, *8*, 4258 (1988). DOI: 10.1063/1.340197
[75] S. Mørup, M.F. Hansen, C. Frandsen. Magnetic Nanoparticles. 2 nd ed. Elsevier Inc. (2018). DOI: 10.1016/B978-0-12-803581-8.11338-4
[76] Y. Yafel, C. Kittel. Phys. Rev. **87**, 290 (1952).
[77] M. Eibschuts, S. Shtrikman. J. Appl. Phys. **39**, 997 (1968).
[78] R.H. Lindquist, G. Constabaris, W. Kundig, A.M. Portis. J. Appl. Phys. **39**, 1001 (1968).
[79] M.A. Polikarpov, V.M. Cherepanov, M.A. Chuev, S.Yu. Shishkov, S.S. Yakimov. J. Phys.: Conf. Ser. **217**, 012115 (2010). DOI: 10.1088/1742-6596/217/1/012115
[80] M.E. Matsnev, V.S. Rusakov. AIP Conf. Proc. **1489**, *1*, 178 (2012).
[81] G.N. Konygin, O.M. Nemtsova, V.E. Porsev. Zhurn. prikl. spektroskopii **86**, *3*, 374 (2019). (in Russian).

Translated by T.Zorina